

# Multiple-damage state retrofit of steel MRFs with composite beams using a minimal-disturbance arm damper

Marzano, Giuseppe A.; Skalomenos, Konstantinos A.; Kurata, Masahiro

DOI:

[10.1061/\(ASCE\)ST.1943-541X.0002697](https://doi.org/10.1061/(ASCE)ST.1943-541X.0002697)

License:

None: All rights reserved

Document Version

Peer reviewed version

Citation for published version (Harvard):

Marzano, GA, Skalomenos, KA & Kurata, M 2020, 'Multiple-damage state retrofit of steel MRFs with composite beams using a minimal-disturbance arm damper', *Journal of Structural Engineering (United States)*, vol. 146, no. 9, 04020169. [https://doi.org/10.1061/\(ASCE\)ST.1943-541X.0002697](https://doi.org/10.1061/(ASCE)ST.1943-541X.0002697)

[Link to publication on Research at Birmingham portal](#)

## Publisher Rights Statement:

This material may be downloaded for personal use only. Any other use requires prior permission of the American Society of Civil Engineers. This material may be found at: [https://doi.org/10.1061/\(ASCE\)ST.1943-541X.0002697](https://doi.org/10.1061/(ASCE)ST.1943-541X.0002697)

## General rights

Unless a licence is specified above, all rights (including copyright and moral rights) in this document are retained by the authors and/or the copyright holders. The express permission of the copyright holder must be obtained for any use of this material other than for purposes permitted by law.

- Users may freely distribute the URL that is used to identify this publication.
- Users may download and/or print one copy of the publication from the University of Birmingham research portal for the purpose of private study or non-commercial research.
- User may use extracts from the document in line with the concept of 'fair dealing' under the Copyright, Designs and Patents Act 1988 (?)
- Users may not further distribute the material nor use it for the purposes of commercial gain.

Where a licence is displayed above, please note the terms and conditions of the licence govern your use of this document.

When citing, please reference the published version.

## Take down policy

While the University of Birmingham exercises care and attention in making items available there are rare occasions when an item has been uploaded in error or has been deemed to be commercially or otherwise sensitive.

If you believe that this is the case for this document, please contact [UBIRA@lists.bham.ac.uk](mailto:UBIRA@lists.bham.ac.uk) providing details and we will remove access to the work immediately and investigate.

# Multi Damage-State Retrofit of Steel Moment-Resisting Frames with Minimal Disturbance Arm Damper

Giuseppe Marzano<sup>1</sup>; Konstantinos A. Skalomenos<sup>2,3</sup>; Masahiro Kurata<sup>3</sup>

<sup>1</sup>*Architecture and Architectural Engineering, Kyoto University, Kyoto, Japan*

<sup>2</sup>*Department of Civil Engineering, School of Engineering Edgbaston, Birmingham, UK*

<sup>3</sup>*Disaster Prevention Research Institute, Kyoto University, Kyoto, Japan*

## ABSTRACT

This study presents a design method for the seismic retrofit and rehabilitation of steel moment resisting frames (MRFs) with composite steel-concrete beams using the Minimal Disturbance Arm Damper (MDAD). The purpose is to enhance the seismic performance of this type of MRF by controlling both the overall structure deformation (roof and story drifts) and damage of individual members (local ductility). The MDAD imposes adequate strength and stiffness to limit the story drifts to the targeted values as well as redistributes the internal forces in order to delay beam yielding and fracture. The proposed design method for seismic retrofit and rehabilitation of MRFs integrates the member's strength and ductility indices, such as the bending moment and plastic rotation, into the global frame response in terms of overall shear capacity and story drift through equations developed based on beam-column theory principles. The proposed design method aims to retrofit the structure to satisfy multiple performance objectives, such as (a) the delay of steel beam yielding, (b) the reduction of beam plastic rotation,

(c) the control of strength reduction in post-fracture behavior, and (d) the recovery of overall shear strength after frame rehabilitation. An experimental campaign was also conducted to evaluate the performance of both retrofitted and bare MRFs. The effectiveness of the proposed retrofit and rehabilitation procedure in limiting the story deformation and improving member ductility of the MRFs as well as its efficiency in recovering the overall strength capacity of heavily damaged framed structures was validated.

**KEYWORDS:** composite steel/concrete beam; multi damage-state; seismic retrofit; post-fracture behavior; experimental validation

## **1. INTRODUCTION**

Steel Moment-Resisting frames (MRFs) are high-performance seismic-resistant structures capable of reaching large deformations without collapsing due to the large ductility of steel material, the superior performance of the MRF as a structural system, and the well-designed connections. The large inherent ductility of steel MRFs allows engineers to adopt large reduction factors as compared to other structures, and therefore, these types of structures can experience multiple damage states during their inelastic response. As a result, the latest seismic design approaches require steel MRFs to satisfy multiple performance objectives, i.e. levels of damage sustained under corresponding levels of seismic hazard, following the concept of Performance Based Seismic Design (PBSD), (Priestley 2000).

For steel MRFs, modern codes such as FEMA-273 (1997), FEMA-351 (2000) and ATC 40 (1996) suggest to check the multiple damage states of the frames mainly through two parameters:

(1) the story drift for controlling the overall frame response (frame limit state) and (2) the beam plastic rotation for controlling the damage in a local level (component limit state).

ASCE 41-13 (2013), complying with the PBSO framework, proposes further developments of the retrofit procedures including intermediate performance levels between the original performance levels, ultimately aiming to increase the safety/assessment limits in terms of story drifts and beam plastic rotations. Several studies have been conducted to identify the effects of the retrofit systems on steel frames under the framework of PBSO. Mirzaee and Estekanchi (2015) proposed a procedure for retrofitting steel frames with shear wall panels or viscous dampers in order to control the overall frame response. Tsai (2012) developed a performance-based approach where steel braces redistribute the forces between the frame elements after the collapse of a column due to accidental loading. Hariri-Ardebili et al. (2014) have proposed an analytical method to obtain the overall response of concentrically braced frames designed in terms of story drift according to the limitations of the performance levels considered. Barroso et al. (2002) evaluated the roof drift and energy dissipation capacity of two steel frames from the SAC Phases II project (1997) retrofitted with friction pendulums, linear viscous dampers, and an active tendon brace system. Additional details about retrofit methods for steel frames are available in Ohata and Toyada (2003). These studies evaluated the overall response of the frame in terms of roof or story drift. However, few studies directly examine the sustained plastic rotation at beam ends, which is one of the two critical indices addressed by PBSO.

Studies that consider the local ductility as a main retrofit parameter have been mainly reported for concrete and steel structures. Bedon and Chisari (2017) have presented a design method for retrofitting concrete structures using Fiber Reinforced Polymers (FRP) where both the local ductility of the concrete elements and overall flexibility of the structure were

considered. For steel MRFs, some well-known retrofit approaches have considered moving the plastic zone far from the critical connection. By implementing this low-disturbance technique with respect to the architectural space, an additional ductility is offered. Some examples of technologies that utilize this approach are the knee-braces (Leelataviwat et al. 2011; Leelataviwat et al. 2017), the improved design of weld access holes in beam-to-column connections (Mao et al. 2004), the concept of reduced-beam-sections (RBS) in beam ends (Chen and Chao 2001) as well as the enhancement of connection performance by adding energy-dissipation devices (Kim and Choi 2006; Benavent-Climent 2011).

Taking advantage of their ductility, steel MRFs can achieve large deformations; however, a concrete floor slab rigidly connected to the top flanges of steel beams, known as a composite steel-concrete beam, increases the strain demand on the bottom flanges of beam ends under positive bending (slab under compression), triggering an early yielding and premature fracture (Ricles et al. 2004). For MRFs with a concrete floor slab, Pellegrino et al. (2009) proposed to strengthen composite beams using FRP technology where the overall frame ductility was enhanced by improving the local ductility of the beams. The present research develops a retrofit procedure to control both the story drift and member ductility, offering an efficient frame upgrade that meets the multiple performance requirements of PBSD and overcomes the deficiencies of current retrofit methods for MRFs. The retrofit system, named the Minimal-Disturbance Arm Damper (MDAD) (Lavan et al. 2017), is designed to enhance the seismic performance of steel MRFs with composite beams by adequately increasing story strength and stiffness and reducing plastic deformation demands at beam ends under positive bending. The basic behavior and design procedures of MDAD, which delay yielding and reduce plastic

rotation under positive bending, have been verified through tests and numerical simulations (Kurata et al. 2016).

In this study, a multi-damage state retrofit procedure for steel MRFs with composite beams is developed with three retrofitting phases defined along with their corresponding damage states. These phases are: (1) the elastic phase where concrete cracking and beam yielding are considered, (2) the plastic phase where concrete crushing and plastic deformation of the steel beam are considered, and (3) the post-fracture phase where multiple fractures in steel beams are considered. More specifically, the MDAD aims to reduce the bending moment demand at the elastic phase and plastic rotation at the plastic phase. After the occurrence of the first beam-end fracture, the design of MDAD aims to prevent the strength deterioration of the frame by compensating for the lost strength. In addition to the three previous retrofit phases, a fourth phase, the rehabilitation phase is proposed which aims to recover the strength and stiffness of the damaged frame . The multi-damage state retrofit procedure combined with the multiple options in retrofitting targets provided by the MDAD enables existing steel MRFs to effectively satisfy the desired performance levels. By controlling both the overall structure deformation and damage on single beam ends a reserve capacity is provided for cases when the seismic demand is higher than or the affordable damage level is lower than those considered during the initial design.

## **OVERVIEW OF THE MINIMAL-DISTURBANCE ARM DAMPER**

First, an overview of the concept and features of MDAD is presented to explain the concept behind the retrofit considering both the local and global performance evaluation parameters. The MDAD is a relatively light retrofit device designed for minimal-disturbance seismic upgrades,

thus saving space for building users. For this purpose, the MDAD is installed above two-thirds of the building height, as shown in Figure 1(a). The MDAD is composed of small-sized steel elements and does not require either heavy construction equipment for installation or special machinery for operation. The MDAD is designed for MRFs with composite beams that suffer premature fractures under positive bending (Leon et al. 1998). The MDAD has been mainly developed for low- and mid-rise commercial buildings and its low-disturbance functionality is beneficial for the continuation of business activities during installation and operation.

The MDAD is comprised of two main elements: bending plates (BP) and tension rods (TR), as shown in Figure 1(a). The bending plates are two steel plates installed at the left and right side near the top of the column, working as fuses to dissipate energy by plastic deformation. Both bending plates are connected with a rigid block at their middle, named as the middle-connecting (MC) block, in order to deform together. Figure 1(b) presents the load-resisting mechanism of the MDAD. Under a lateral force, the deformation of the beam-column connection imposes a load on the tension rod. Due to the MC block and the use of a slotted hole at the connection with the beam's bottom flange, the tension rods sustain tension force only. Thus, slender elements can be used for the tension rods while a stable bilinear hysteresis is provided through the yielding of the bending plates in both directions.

The difference in the behaviors of the MDADs at the interior and exterior column was studied carefully in Zhang et al (2018). The MDAD at the interior column exhibits a stable bilinear hysteresis but the MDAD at the exterior column presents a ratcheting behavior. The ratcheting behavior occurred as the bending plates only bent in one direction. The tension rod started to sustain compression after 2.0% story drift when the end of the tension rod pressed against the pin on the beam after used up the clearance made by the long-slotted hole.

Knee-braces could be considered as similar retrofit systems that respect the above-mentioned features. However, to reach a stable energy dissipation with knee braces, either stocky elements are required, imposing a large stiffness compared to the existing beam ends, or the bottom flange of the beam needs to be cut to increase the demand on the braces (Aristizabel-Ocha 1986).

The MDAD is designed to reduce the rotation demand at the beam ends of the MRFs as well as gently increase the stiffness and strength of the story. Figure 1(c) shows the mechanism by which the MDAD reduces the positive moment at the beam ends and delays the beam yielding. Accordingly, the positive plastic rotation at the beam hinge is reduced. The vertical component of the force adds negative moment at both beam ends. The negative moment and rotation increments can be sustained by the composite beam since it usually has a 1.5-2.0 times larger rotation capacity under negative bending than under positive bending moment (Chung et al. 2011). The design procedure for yielding delay, plastic rotation reduction, and increase of the story stiffness and strength by the MDAD has been verified by testing a one-story two-span MRF (Zhang et al 2018).

## **MULTI DAMAGE-STATE RETROFIT**

The proposed multi damage-state retrofit method controls both the beam plastic rotation and story drift. Figure 2(a) presents the design targets of the three retrofit phases in a frame pushover curve: (a) Phase A for yielding delay, (b) Phase B for fracture delay, and (c) Phase C for the delay in the shear capacity reduction. These phases are related to the performance levels specified in the PBSO framework: Fully Operational, Operational, Life Safe, and Near Collapse. Furthermore, Figure 2(b) illustrates the design target of Phase D, which corresponds to the rehabilitation phase and aims to recover the lateral frame capacity after the frame has experienced heavy damage.



Phase A is a force-based design phase that reduces the positive bending moment at the beam ends. Phase B is a deformation-based design phase and aims to extend the overall deformation capacity of the frame by reducing the positive plastic rotation at the beam ends. Phase C aims to maintain the strength capacity of the frame after deterioration occurs in the beams. The lateral strength of the frame is maintained by delaying the occurrence of fracture and through the complementary strength and stiffness provided by the MDAD.

Phase D aims at improving the seismic performance of an already damaged structure (Suzuki et al. 2017) against subsequent or future earthquakes by taking advantage of the replaceable fuses in the MDAD. The bending plates, after reaching a large deformation during the first seismic event, are replaced with thicker plates to recover the frame lateral strength and stiffness losses from damage that occurred along the frame. The original strength and stiffness of the frame are not exceeded by adding the new fuse elements while the deformation capacity is appreciably increased.

## **RETROFIT PHASE DESIGN**

The design of the phases begins by setting the local response target for the beam end. The target value is inserted in the design equation to calculate the story drift or lateral strength of the frame as a global response. The design equations are developed using the principle of virtual work, where the shear deformation is neglected.

After fracture, the mechanical properties of the beam are affected. The damage parameter  $\omega$  is defined as the ratio between the residual moment capacity after fracture and the initial positive plastic moment of the composite section. Assuming that the damage is initiated at the bottom flange and propagates to the steel web, the corresponding reduction of the moment of inertia of the composite section is estimated.

## Phase A

The elastic properties of the frame are considered in Phase A. The retrofitting local target is a reduction of the positive moment at the beam end and the global target is a delay in yielding from 0.5% story drift to 0.75%. Figure 3(a) shows the pushover curve, with the black lines representing Phase A. In the retrofitted curve, the stiffness changes when the bending plates yield in the MDAD. The bending plate yielding is designed to occur before the beam end yielding. Figure 3(b) shows the moment-rotation relationship of the beam end, where both moment and rotation decrease due to the MDAD retrofitting. Figure 3(c) shows the expected trend of the positive moment against the story drift with and without retrofitting. The moment at the same drift decreases and the yielding is delayed.

The design equation is derived applying the principle of virtual work on the subassembly extracted from the upper floors of the frame, composed of two half-length columns and one beam. For the first floor, the equations need to be modified to account for the rotations at the column bases. The modifications required for the design equation were studied previously in Zhang et al. (2018). The equation is derived as the ratio between the positive beam bending moment with and without retrofitting, or  $R_A$ . By entering the target drift in Equation 1 and considering  $R_A = 1$ , the retrofitted force  $F_d$  is obtained. An equivalent procedure would be to impose a positive beam moment reduction of 15% and calculate the required retrofit force at 0.5% story drift. Finally, additional stiffness induced by the MDAD is controlled so that the overall dynamic characteristics of the MRF are maintained.

$$R_A = \frac{M_{left}}{M_{left,w/o}} = \frac{A \times \delta + B \times F_d + C \times M_{right}}{A \times \delta + C \times M_{right}} \quad [1]$$

Where  $M_{left}$  and  $M_{left,w/o}$  are the positive moments at the left beam end with and without the MDAD. The coefficients  $A$ ,  $B$ , and  $C$  in Equations 2, 3, and 4, are obtained by applying a unit

lateral force at the top of the column, combined with the tension rod force  $F_d$  and the negative bending moment  $M_{right}$ , respectively.  $H$ ,  $L$ ,  $E$ ,  $I_b$ ,  $I_c$ ,  $k$ ,  $e$ , and  $a$  are the specimen height, the specimen span length, the steel elastic modulus, the beam and column moments of inertia, the ratio between the composite and bare moments of inertia of the beam, the eccentricity between the tension rod connection at the beam side and the beam centerline, and the length of the concrete slab under compression, respectively.

$$A = \frac{1}{\frac{H}{12EI_c} + \frac{L(2-a)^3}{24EI_b} + \frac{La(a^2 - 12a + 24)}{24kEI_b}} \quad [2]$$

$$B = A \left[ \left( \frac{H^2}{384EI_c} + \frac{HL}{96EI_b} - \frac{Le}{24EI_b} + \frac{Le}{12kEI_b} + \frac{7HL}{96kEI_b} \right) \cos\alpha - \frac{L^2}{24EI_b} \left( \frac{1}{2} + \frac{1}{k} \right) \sin\alpha \right] - \frac{H \cos\alpha}{4} \quad [3]$$

$$C = \left( \frac{La}{2EI_b} \right) A - 1 \quad [4]$$

Equations 2 to 4 consider the length of the concrete slab under compression based on the properties of the concrete and the section geometry. Figure 3(d) illustrates a schematic of the substructure model with the MDAD used to derive the design equation for Phase A, with different arrows used for internal and external forces.

### **Phase B**

The plastic rotation  $\theta_p$  is used as an index to evaluate the damage at the beam end during Phase B. The targeted reduction of plastic rotation is 20% to delay fracture from 2.0% story drift to 3.0% story drift. The MDAD retrofit force  $F_d$  required to achieve the target is calculated by Equation 5. The ratio between the plastic rotation with and without the MDAD, or  $R_B$ , is set as 0.8 at 2.0% story drift to calculate  $F_d$ . The fracture delay is found by setting  $R_B$  equal to 1. The

design is limited by the increment of the negative plastic rotation at the opposite beam end. Equations 6 to 8 define the coefficients of equation 5.

Figure 4(a) shows the pushover curve of the specimen with Phase B underlined using black lines for the bare and retrofitted configurations. Figures 4(b) and 4(c) show the beam moment-rotation relationship and the positive plastic rotation-drift relationship. The bare and retrofitted lines of Figure 4(c) start at different drifts due to the delay of yielding in Phase A. The positive plastic rotation is also reduced by the amount of plastic deformation sustained by the bending plates after yielding.

The design Equation 5 for Phase B is obtained from the model of Figure 4(d). The moments at the beam ends are released and replaced by internal pins, adding the plastic moments of the sections with and without slab effect,  $M_{p,left}$  and  $M_{p,right}$ , as described in Equations 6 to 8

$$R_B = \frac{\theta_{p,MDAD}}{\theta_p} = \frac{A \times M_{p,left} + B \times F_d + C \times M_{p,right} + \delta}{A \times M_{p,left} + C \times M_{p,right} + \delta} \quad [5]$$

$$A = \frac{(k+7)L}{24EI_b} + \frac{H}{12EI_c} \quad [6]$$

$$B = - \left[ \left( \frac{H_1^3}{6EHI_c} - \frac{H_1^2}{4EI_c} + \frac{H_1H}{12EI_c} \right) \cos\alpha - \frac{(2t^3 + 6t^2 + 6t - 16k + 18)L \cos\alpha + (5 - 3t^3 - 9t^2 - 9t - 8k)L^2 \sin\alpha}{48EI_b k(t+1)^3} \right] \quad [7]$$

$$C = \frac{(k+1)LH}{12EI_b} - \frac{H^2}{12EI_c} \quad [8]$$

Where  $\theta_p$ ,  $H_1$ , and  $t$  are the beam (left end) plastic rotation, the distance of the bending plates centerline from the beam centerline, and the ratio between the composite and steel plastic moments under positive bending.

### **Phase C**

Phase C is intended to delay the deterioration of lateral strength and to reduce the amount of strength reduction after fracture occurs. In this design, the target is to maintain the maximum

lateral strength after fracture occurs until 3.5% story drift. Figure 5(a) shows the pushover curves of the bare and retrofitted frame. Phase C starts at 3.0% story drift when the first fracture of the beam bottom flange is expected and finishes when the frame capacity is reduced below 80%. The fracture delay shown in Figure 5(a) is due to Phase B and no stiffness degradation is expected until 3.5% story drift. Figure 5(b) represents the force sustained by the tension rod when fracture occurs at the beam-end. At the onset of fracture, the force sustained by the tension rod compensates for the strength lost from the fractured beam bottom flange and maintains the overall lateral strength capacity of the frame. As shown in Figure 5(c), the MDAD provides lateral stiffness against the opening of the beam-column connection and thus the frame capacity after fracture increases.

The parameters that control the response of the beam ends under positive and negative moments during phase C are the damage parameters  $\omega^+$  and  $\omega^-$ , respectively defined in Equations 9 and 10. The relationships shown in Figure 6(a) and 6(b) demonstrate the correlation between the beam parameters and the damage factors. In Figure 6(b), the first change of slope corresponds to the full damage of the bottom flange. The value of 0.6 is assumed as a limit for the retrofitting and corresponds to a beam section with both the bottom flange and 20% of the web length being fully damaged. After the limit value is reached, the retrofit is assumed no longer effective due to most of the steel section being damaged; however, for completeness, the relationship is shown until 1.0. The letter  $f$  indicates the beam properties calculated in the fracture configuration.

$$\omega^+ = 1 - \frac{M_{p,left}^f}{M_{p,left}} [9]$$

$$\omega^- = 1 - \frac{M_{p,right}^f}{M_{p,right}} [10]$$

Design Equation 11 is used to find the ratio between the shear force with and without retrofitting,  $R_C$ . The retrofitted force is calculated at the drift limit of 3.5%, as mentioned above. The updated beam parameters after section reduction are calculated and added in Equations 12-14 to determine the response of the frame. The equations are derived on the basis of the model shown in Figure 5(c), which is identical to that of Design Phase A with the exception that beam fractures are considered.

$$R_C = \frac{V_{MDAD}}{V} = \frac{A' \times \delta + B' \times \omega^- M_{p,R} + C' \times F_d}{A \times \delta + B \times \omega^- M_{p,R}} \quad [11]$$

$$A = \frac{3E}{H} \left( \frac{1}{\frac{H}{4I_c} + \frac{L}{I_b}} \right); \quad A' = \frac{3E}{H} \left( \frac{1}{\frac{H}{4I_c} + \frac{L}{I_b^f}} \right) \quad [12]$$

$$B = A \frac{L}{2EI_b}; \quad B' = A' \frac{L}{2EI_b^f} \quad [13]$$

$$C' = A' \left\{ \left[ \frac{H^2}{96EI_c} - \frac{L}{12EI_b^f} \left( \frac{e}{2} + H \right) \right] \cos \alpha + \frac{L^2}{16EI_b^f} \sin \alpha \right\} \quad [14]$$

### **Phase D**

Phase D aims to provide a temporary, but rapid recovery of the frame lateral strength capacity after a strong earthquake to prevent structure collapse under subsequent earthquakes. Figure 2(b) represents the rehabilitation phase along the pushover curve. In this design example, the target is to recover the lateral strength of the frame above 80% of the base shear of the un-retrofitted frame (250 kN) reached under the story drift of 3.5%. The design equations are the same as those in Design Phase C; however, the design phase starts from the residual drift, equal to 1.5%. The residual drift of Phase C is calculated by dividing the frame lateral force with the stiffness reduced by  $\omega$ , which is between 0.2 and 0.3. The total displacement of the frame during Phase D is 2.0% story drift, from 1.5% to 3.5% story drift.

In practice, the damage parameter  $\omega$  can be determined after inspecting the actual damage at the beam ends. For this design example, if the damage reduces the lateral strength more than 20%, rehabilitation is required.

## TEST SETUP

### *Specimen and test setup*

Figure 7(a) shows the schematic view of the test specimen. The specimen represents a half-scaled one-story two-span substructure extracted from a mid-floor of a typical Japanese steel MRF. The overall size is 6,000 mm long and 1,650 mm high. Columns 1-3 are made of HSS-175 mm  $\times$  175 mm  $\times$  12 mm sections and Beams 1-2 are made of I-200 mm  $\times$  100 mm  $\times$  5.5 mm  $\times$  8 mm sections. The beam-to-column strength ratio is around 2.0. The columns are pin-supported at the bottom ends and connected with each other at the top with rigid trusses made of round HSS 165 mm  $\times$  12 mm sections to impose equal displacements. Gusset plates with a 12 mm thickness are used to simulate pinned behavior at the truss ends. The beam-column connection is a through-diaphragm type where short brackets are shop-welded to the columns. A concrete slab of 500 mm  $\times$  65 mm was cast for a length of 920 mm on each beam side. The slab-beam connection is designed rigid, using one row of shear connectors welded to the beam flange every 75 mm. Due to the size limitation for headed studs, M10 high strength bolts with 40 mm length are used. The slab is designed to increase the beam strength,  $M_p$ , of the bare steel section by 30% and the bending stiffness by 80% under a positive bending moment. The out-of-plane displacement of the specimen is restrained at Column 1 and 3 using two restrainers. The specimen is subjected to a quasi-static loading using two hydraulic jacks: Jack 1 with a 500 kN capacity is connected to Column 1 and Jack 2 with a 200 kN capacity is connected to Column 3.

Jack 1 is displacement controlled, while Jack 2 automatically applies an equal but opposite in sign force.

Figure 7(b) shows the internal column and connection retrofitted with the MDAD. The bending plates are bolt-connected at the edges to a rectangular frame comprised of four spacing plates that are firmly attached on the column. The plates are constrained to sustain the same horizontal deformation by the mid-connector. The tension rods are pin connected to the bending plates. The connection between the tension rods and the beam bottom flanges is made by a clevis with a slotted hole that allows the rods to slide, thus avoiding compression.

Table 1 summarizes the design drift, target local parameters, and the thicknesses of the bending plates required for each phase, computed based on the proposed design procedure. The MDAD retrofitting system is installed at all the columns, 400 mm below the beam center line. It was chosen to use two sets of bending plates. The bending plate is 12 mm thick and 240 mm  $\times$  375 mm for Phases A to C, and 16 mm thick and 240 mm  $\times$  375 mm for Phase D. The diameter and length of the tension rods are 30 mm and 1,245 mm, respectively. Table 2 summarizes the material properties of the beam web and flange, concrete, and bending plate, as obtained from coupon tests.

### ***Measurement system***

The strain gauges (SG) and displacement transducers (DT) are installed as illustrated in Figure 8. The strain gauges are used to calculate the forces in the elements composing the specimen. Eight strain gauges are attached to each column, four above and four below the beam, at the front and back column faces. The columns are designed to remain elastic during the entire test, so the strain responses are used to calculate the shear and moment along with the elements.



The same procedure is used for the beams in the elastic range. The strain gauges are attached to six sections along the beams: four inside the composite section length and two outside. The neutral axes at the composite sections are estimated, and the progress of concrete slab cracking is evaluated. Two displacement transducers are installed at the top of Column 1 and 3 to measure the displacement of the external columns and the story drift. Eight displacement transducers are installed at the beam ends to estimate the beam end rotation.

### ***Loading Protocol and Retrofitting Installations***

Figure 9 presents the loading protocol used in the test. The protocol was designed to evaluate the effects of the retrofit at each phase. In Phase A, the 0.5% and 0.75% loading cycles were repeated in both the bare and retrofitted configurations to estimate the positive moment reduction at the beam ends, the increment in the frame stiffness, and the delay of yielding. In Phase B, the loading cycles of 1.0% and 1.5% story drifts were repeated first on the bare specimen and then on the retrofitted specimen to evaluate the post-yielding stiffness of the frame, the maximum lateral strength, and the fracture delay. The cyclic loading continued on the retrofitted specimen until the first fracture occurred at the first loading cycle of 3.0% story drift as expected by design. Phase B ended after the fracture. The retrofit system was removed, and the specimen was loaded for a half cycle from the residual drift to a 3.5% story drift to evaluate the residual lateral strength with one out of four beam ends fractured. Then, the retrofit system for Phase C was reinstalled, and the loading was continued until the lateral force was reduced below 80% of the maximum value. Finally, Phase D loading started with the residual drift after the half cycle of the bare configuration. The bending plates were replaced, and the loading was continued until a 4.0% story drift.

## TEST RESULTS

### *Overall behavior*

The retrofitted frame demonstrated stable behavior until the end of loading. Figure 10 shows the specimen and the hysteresis behavior of the frame in terms of the drift and lateral strength relationship. Table 3 summarizes the primary parameters in the hysteresis behaviors of the bare and retrofit configurations. The elastic stiffness and the yielding strength in Phase A increased by 15%. In Phase B, the post-yielding stiffness increased by 46% due to the delay of the yielding of each single beam end in conjunction with the stiffness added by the MDAD. The maximum lateral strength of the retrofitted frame was 320 kN, which is 28% larger than that of the original frame. In Phase D, the residual stiffness and strength increased by 23% and 52%, respectively, by rehabilitating the damaged frame.

Table 4 lists the main loading points during the tests. The letters *B* and *R* indicate the bare and retrofitted configuration, respectively. Note that in Phase A and B the retrofitted configuration was tested, with some damage occurring during the testing of the bare configuration. In the bare configuration (B1), the first yielding occurred at the bottom flange of the left end of beam 1 (B1L) at a 0.5% story drift. In the retrofit configuration, all the beam ends yielded at a 1.0% story drift (R1). In Phase B and C, the first and second fractures in the retrofit configuration occurred at 3.0% and 3.5 % story drifts, respectively (R2, R3). For the Phase D validation, the residual strength was obtained and compared only in the positive loading direction (B3 and R5) because the retrofit system failed during the negative loading cycle of the 3.5% story drift. The bolt connecting the bending plates to the mid-connector at the external Column 3

yielded. The failure of the retrofit system caused a drop in the force sustained by the tension rod and consequently a drop in the lateral strength in the specimen.

The global phase targets were achieved in the test, confirming the validity of the multi damage-state retrofit design procedure for improving the overall response of a steel MRF by controlling the local response parameters. The details of the local parameters at each phase are discussed in the following sections.

### ***Phase A results***

In the Design Phase A, the global target of delaying the yielding from a 0.5% to 0.75% story drift was achieved. Figure 11(a) shows the lateral force-story drift relationship of the frame and presents a 15% increase of the frame stiffness. Figure 11(b) shows the positive moment-story drift relationship at the left beam ends of Beam 1, which corresponds to Figure 3(c). The bending moment was reduced successfully by the retrofit. Table 5 summarizes the local parameters. At a 0.75% story drift, the positive moment at the Beam 1 left end (B1L) and the left end of Beam 2 (B2L) were reduced by 14% and 18%, respectively, satisfying the design target of a 15% reduction. The effect of composite action by the floor slab varied by the beam ends, i.e., the composite factor  $k$  was 2.3 and 1.9, respectively. In summary, two out of four beam ends yielded at a 0.75% story drift and the other beam ends yielded at a 1.0% story drift. The further delay in the yielding was due to the use of 12 mm thick bending plates instead of the 9 mm thick plates required from the design procedure.

### ***Phase B results***

In Design Phase B, the global target of delaying the fracture from 2.0% to 3.0% story drift was achieved. The first fracture occurred at a 3.0% story drift at the bottom flange of B2L, as expected from the loading protocol. The second fracture occurred at the first loading cycle of - 3.5% story drift at the top flange of the left end of Beam 1(B1L). The observed fracture sequence is important for evaluating the effects of the retrofit system to the beam ends. Figure 12(a) shows the hysteresis behavior of the frame in the bare and retrofitted configurations during 1.0% and 1.5% loading cycles. The figure shows a clear difference in the post-yielding stiffness after a 0.75% story drift. Figure 12(b) shows the relationship between the story drift and the positive plastic rotation at B1R. This plot corresponds to the concept shown in Figure 4(c).

Table 6 summarizes the elastic and post-yielding stiffnesses of the specimen. The elastic stiffness identified during the 1.0% cycles in the two configurations were similar with a difference of 5%; however, after yielding the difference increased to around 10% due to the increased damage after the 1.5% loading cycle for the bare configuration. The difference in the post-yielding stiffness was around 45%. The stiffness provided by the MDADs improved the post-yielding stiffness of the frame to a value almost equal the elastic stiffness until a 1.5% story drift.

Table 7 summarizes the plastic rotation at the right and left ends of Beam 1. The rotation of the left side is larger than the right side due to the different stiffness between the internal and external joints. At 1.5% story drift, the average positive plastic rotation reduction was 19%, a value close to the local target of 20%. The plastic demand is shown as the ratio between the cumulative plastic rotation and the yielding rotation, with the average reduction between the two beam ends due to the MDAD being 26%.

Table 8 shows the crack width in the concrete slab measured at the B2L side approximately 200 mm away from Column 2 face. The crack width decreased due to the retrofit, with the reduction increasing from 43% to 71% as the story drift increased. The reduction indicates the decrease of the rotation of the beam ends and the beam curvature near the beam-column connections.

### ***Phase C results***

Figure 13 shows the hysteresis behavior of the retrofitted configuration during the loading cycle of 3.0% and 3.5% story drifts. The 3.5% cycle of the bare frame is added for comparison, including the same number of fractures as the retrofitted frame. The first fracture occurred at B2L during the first cycle of the 3.0% story drift. The force in the TR3 increased by 20% to compensate for the fracture at the bottom flange. Due to the backup strength mechanism provided by the MDAD, the frame lateral strength remained at 350 kN even after beam fracture. The strength deterioration started when multiple beam fractures occurred after reaching the loading cycle of 3.5% story drift. The frame capacity at the end of the phase was 270 kN, 23% lower than the design value of 350 kN. The capacity was lower than the design value due to the 12 mm thickness plate used in Phase C instead of the 16 mm required by the design procedure. According to the design equation of Phase C, the use of a 12 mm thick plate targets a lateral strength reduction of 15% or 297 kN, close to the reduction observed at 3.5% drift.

Under large displacement, the beam bottom flanges are expected to suffer local damage under negative bending, in addition to the further negative moment applied by the retrofit system. During the test, however, no local buckling was detected. This phenomena is due to the horizontal component of the MDAD force,  $F_d \cos \alpha$ , which acts as a concentrated force applied at

the middle of the beam length in the clevis connecting the beam to the tension rod. This force is always opposite to the direction of the external load adding compression to the bottom flange of the beam section under positive bending and tension to the bottom flange of the section under negative bending. The tensile force reduces the compression at the bottom flange, thus delaying the onset of local buckling. Figure 14 shows the BIL bottom flange strain under negative moment in the bare and retrofitted configurations. The strain values are similar in the early stage, however, after yielding, the strain under compression at the bottom flange starts to reduce significantly with the retrofit system. In the retrofitted configuration, at -3.0% story drift the strain in the bottom flange under negative moment is 64% of the strain in the bare configuration.

#### ***Phase D results***

Figure 15 shows the force-story drift relationship before and after the rehabilitation using the 16 mm thick bending plates. At the design target drift of 3.5%, the bare frame sustained only 165 kN, 66% of the maximum lateral strength. The rehabilitated frame sustained 233 kN, 93% of the bare frame's maximum lateral strength, achieving the design rehabilitation target for the lateral strength of over the 80% of the bare maximum lateral strength. The frame strength with the retrofit increased until a 4.0% story drift and reached 250 kN, which is 100% of the bare lateral strength. The ultimate capacity of the rehabilitated configuration was not identified due to bolt failure in the MDAD.

The frame stiffness between the bare, retrofit, and rehabilitated configurations are compared in Table 9. The bare frame stiffness decreased by 15% after the first fracture and by almost 50% after three out of four beam ends fractures. The stiffness reduction in the rehabilitated frame was only 4.2% and 6.3% of the elastic value with one and three out of four beam end fractures,

respectively. At this point, the retrofit system provided most of the lateral strength. At 3.5% story drift, the slab separation from the column face was 16 mm for the bare configuration while in the rehabilitated configuration the separation was 9 mm. A similar reduction was observed for the crack openings in the concrete slab.

Two failure mechanisms of the retrofit system elements were observed during the ultimate stage of the frame test: buckling of the external tension rods (TR1 and TR4) due to the ratcheting behavior and yielding of the bolt connecting the bending plate to the mid-connector in TR4. While the pins connecting the end of the tension rods and the clevis were designed to slide in the slotted hole, the vertical component of the retrofitting force,  $F_d \sin \alpha$ , increased the friction in the slotted hole and restrained the smooth movement of the pins. Additionally, the sudden failure of the bolt in the mid-connector (TR4) was observed. Both failures occurred at a story drift larger than those considered in the design; however, the failure mechanism can be improved in the design stage of the MDAD elements and connections. This is a subject of future study.

## **Conclusions**

The proposed multi damage-state retrofit procedure aims to advance the retrofitting of steel moment resisting frames by giving more attention to the behavior of the composite beams. The procedure focuses on the retrofitting of the beam ends, considered critical parts of a frame during a seismic event. Three damage states experienced by the beam end are evaluated: yielding, fracture, and post-fracture. The goal is to control both the local beam end and the global frame responses to effectively satisfy the corresponding performance levels. The retrofit design also includes a rehabilitation phase for a temporary and rapid recovery of the frame performance after a significant seismic event. The design equations that fulfill the above design methodology were derived for the Minimal Disturbance Arm Damper (MDAD). A quasi-static test on a half-scale

one-story two-span steel frame retrofitted with the MDADs was conducted to validate the accuracy of the design methodology. The main findings are as follows:

- For each retrofit phase, the subassembly model used to derive the analytical equation that correlates the story drift and local response parameters of the beam end was identified and the design equations derived. The forces required by the MDAD for the retrofitting were obtained by substituting the story drift of interest and the targeted reduction in local response parameters.
- In the verification test, the retrofit system reduced the positive bending moment at the beam ends by 16% in the elastic phase and delayed yielding from a 0.5% to a 0.75% story drift. In the plastic phase, the MDAD reduced the positive plastic rotation at the beam ends by 17% and delayed the onset of the beam bottom flange fracture from a 2.0% to a 3.0% story drift. These improvements were close to the design targets of 15% positive moment reduction and 20% plastic rotation reduction. The frame shear capacity had no reduction even after the first fracture of the beam bottom flange. The start of the stiffness deterioration was delayed from a 3.0% story drift to a 3.5% story drift.
- The rehabilitation with a stronger retrofit configuration recovered the shear strength to 96% of the maximum shear capacity. The frame capacity continued to increase until the end of loading. At 4.0% story drift, the retrofitted frame recovered 100% of the shear capacity even with three out of four beam-ends fractured.
- While not explicitly considered in the design, other local damage was also reduced by the MDAD. The crack widths in the concrete floor slab were reduced by 60%-70% at story drifts of 1.0%-1.5%. The bottom flange strain at the beam-ends was reduced by 36% under negative bending, which inherently delayed the initiation of local buckling.



## **Data availability**

Some or all of the data, models, or code generated or used during the study are available from the corresponding author by request (list items).

- measurement data from test

## **Acknowledgments**

The authors would like to gratefully acknowledge the generous support offered by the Japan Iron and Steel Federation. Additional support was provided by JSPS KAKENHI Grant Number 16H06108. The guidance provided by Prof. Yoshiki Ikeda of Kyoto University was invaluable. The support of Yuga Sasaki of Kyoto University in the experimental work is truly appreciated.

## **REFERENCES**

- Aristizabal-Ochoa, J. D. (1986). "Disposable Knee Bracing: Improvement in Seismic Design of Steel Frames." *J. Struct. Eng.*, 112(7), 1544-1552.
- ASCE (American Society of Civil Engineers). (2013). "Seismic Evaluation and Retrofit of Existing Buildings." *ASCE 41-13*, SEAOC Convention proceedings, California.
- ATC (Applied Technology Council). (1996). "Seismic Evaluation and Retrofit of Concrete Buildings." *ATC-40*, Redwood city, California.
- Barroso, L. R., Breneman, S. E., and Smith, H. A. (2002). "Performance Evaluation of Controlled Steel Frames under Multilevel Seismic Loads." *J. Struct. Eng.*, 128(11), 1368-1378.
- Benavent-Climent, A. (2011). "An energy-based method for seismic retrofit of existing frames using hysteretic dampers." *Soil Dynamics and Earthquake Engineering*, 31(2011), 1385-1396.

- Chen, S., and Chao, Y. C. (2001). "Effect of composite action on seismic performance of steel moment connections with reduced beam sections." *Journal of Constructional Steel Research*, 57(2001), 417-434.
- Chisari, C., and Bedon, C. (2017). "Performance-based design of FRP retrofitting of existing RC frames by means of multi-objective optimisation." *Bollettino di Geofisica Teorica ed Applicata*, 58(4), 377-394.
- Chung, Y-L., Nagae, T., Matsumiya, T., Nakashima, M. (2011). "Seismic resistance capacity of beam-column connections in high-rise buildings: E-defense shaking table test." *Earthquake Engineering & Structural Dynamics*, 40(6), 605-622.
- FEMA (Federal Emergency Management Agency). (1997). "NEHRP Guidelines for the Seismic Rehabilitation of Buildings." *FEMA-273*, Washington, DC.
- FEMA (Federal Emergency Management Agency). (2000). "Recommended Seismic Evaluation and Upgrade Criteria for Existing Welded Steel Moment-Frame Buildings." *FEMA-351*, Washington, DC.
- Hariri-Ardebili, M. A., Sattar, S., and Estekanchi, H. E. (2014). "Performance-based seismic assessment of steel frames using endurance time analysis." *Engineering Structures*, 69(2014), 216-234.
- Kim, J., and Choi, H. (2006). "Displacement-Based Design of Supplemental Dampers for Seismic Retrofit of a Framed Structure." *Journal of Structural Engineering*, 132(6), 873-883.
- Kurata, M., Sato, M., Zhang, L., Lavan, O., Becker, T., and Nakashima, M. (2016). "Minimal-disturbance seismic rehabilitation of steel moment-resisting frames using light-weight steel elements." *Earthquake Engineering & Structural Dynamics*, 45, 383-400.
- Lavan, O., Sato, M., Kurata, M., Zhang, L. (2017). "Local Deformation Based Design of Minimal-Disturbance Arm Damper for Retrofitting Steel Moment-Resisting Frames." *Earthquake Engineering & Structural Dynamics*, 46(9), 1493-1509.
- Leelataviwat, S., Doung, P., Junda, E., and Chan-anan, W. (2017). "Ductile Knee-Braced Frames for Seismic Applications." *International Conference on Earthquake engineering and Structural Dynamics*, Reykjavik, Iceland.
- Leelataviwat, S., Suksan, B., Srechai, J., and Warnitchai, P. (2011). "Seismic Design and Behavior of Ductile Knee-Braced Moment Frames." *Journal of Structural Engineering*, 137(5), 579-588.
- Leon, R. T., Hajjar, J. F., Gustafson, M. A., (1998). "Seismic Response of Composite Moment-Resisting Connections. I: Performance." *Journal of Structural Engineering*, 124(8), 868-876.

- Mao, C., Ricles, J., Lu, L., and Fischer, J. (2001). "Effect of Local Details on Ductility of Welded Moment Connections." *Journal of Structural Engineering*, 127(9):1036-1044.
- Mirzaee, A., and Estekanchi, H. E., (2015). "Performance-Based Seismic Retrofitting of Steel Frames by the Endurance Time Method." *Earthquake Spectra*, 31(1), 383-402.
- Ohata, M., and Toyoda, M., (2004). "Damage concept for evaluating ductile cracking of steel structure subjected to large-scale cyclic straining." *Science and Technology of Advanced Materials*, 5(2004), 241-249.
- Pellegrino, C., Maiorana, E., and Modena, C. (2009). "FRP strengthening of steel and steel-concrete structures: an analytical approach." *Materials and Structures*, 42, 353-363.
- Priestley, M. J. N., (2000). "Performance Based Seismic Design." 12<sup>th</sup> World Conference on Earthquake Engineering, Auckland, New Zealand.
- Ricles, J. M., Zhang, X., Lu, L., and Fisher, J., (2004). "Development of Seismic Guidelines for Deep-Column Steel Moment Connections." ATLSS National Center for Engineering Research on Advance Technology for Large Structural Systems, ATLSS Report No. 04-13, Bethlehem, PA.
- Sommerville, P., Smith, N., Punyamurthula, S., and Sun, J. (1997). "Development of ground motion time histories for phase II of the FEMA/SAC steel project." SAC Background Document, Rep. No. SAC/BD-97/04.
- Suzuki, W., Aoi, S., Kunugi, T., Kubo, K., Morikawa, N., Nakamura, H., Kimura, T., and Fujiwara, H. (2017). "Strong motions observed by K-NET and KiK-net during the 2016 Kumamoto earthquake sequence." *Earth, Planets and Space*, December 2017, 69:19.
- Tsai, M. (2012). "A performance-based design approach for retrofitting regular buildings frames with steel braces against sudden column loss." *Journal of Constructional Steel Research*, 77(2012), 1-11.
- Zhang, L., Marzano, G., Sasaki, Y., Kurata, M., Skalomenos, K. (2018). "Force redistribution of steel moment-resisting frame retrofitted with a minimal disturbance arm damper." *Soil Dynamics and Earthquake Engineering*, 114 (2018), 159-173.

**Table 1.** Plate thicknesses for phase targets.

	Phase A	Phase B	Phase C	Phase D
Drift [%]	0.75	3.0	3.5	4.0
Design targets	-15% $M_y^+$	-20% $\theta_p^+$	-0% V	> 80% $V_{bare,max}$
Design Plate [mm]	10	12	16	16
Plate tested [mm]	12	12	12	16

**Table 2.** Material properties.

	$\sigma_y$ [MPa]	$\sigma_u$ [MPa]	$E$ [MPa]
Flange	301	423	203,000
Web	372	441	204,000
Slab	24	32	24,808
Bending plate	311	450	217,000

**Table 3.** Overall frame behavior.

	Bare	Retrofit	ratio
Elastic stiffness [kN/mm]	9.6	11.0	1.15
Yielding force [kN]	119	136	1.14
Second stiffness [kN/mm]	5.0	7.3	1.46
Maximum strength [kN]	250	320	1.28
Residual stiffness with fracture [kN/mm]	7.3	9.0	1.23
Residual strength with fracture [kN]	165	250	1.52

**Table 4.** Main loading points during testing.

Number	Phase	Loading Cycle (Drift)	Event
B1	A	0.50%	First beam end yielding (B1L, bottom)
R1	A to B	1.00%	Four beam ends yielding
R2	B to C	3.00%	First fracture (B2L, bottom)
B2	B	2.00%	Bare frame 1 <sup>st</sup> fracture
B3	C	1.65%	Residual drift
R3	C	-3.50%	Second fracture (B1L, top)
R4	D	-3.50%	MDAD failure (TR4)
B4	D	3.50%	Residual capacity
R5	D	4.00%	Recovered capacity

**Table 5.** Phase A: beam rotational stiffness and strength.

Target 15% drift [%]	section	$K^+$ [kNm/rad]	$K^-$ [kNm/rad]	$k$	$M^+$ [kNm]		Reduction
					Bare	MDAD	
0.75%	B1L	15,979	8,284	2.3	41	35	14%
	B2L	20,922	9,063	1.9	33	27	18%

**Table 6.** Frame stiffnesses.

Drift [%]	Configuration	$K$ [kN/mm]	Ratio	$K_{sec}$ [kN/mm]	Ratio
1.0	Bare	9.9	—	—	—
	Retrofit	9.4	0.95	—	—
-1.0	Bare	9.9	—	—	—
	Retrofit	9.5	0.97	—	—
+1.5	Bare	10.0	—	5.0	—
	Retrofit	8.7	0.87	7.3	1.45
-1.5	Bare	8.9	—	5.5	—
	Retrofit	7.9	0.88	7.5	1.36

626

**Table 7.** Plastic rotation.

Drift	Section	$\theta_p$ [rad]			$\Sigma \theta_p / \theta_y$		
		Bare	MDAD	Red.	Bare	MDAD	Red.
1.5%	B1L	0.0070	0.0057	19%	11.0	7.7	30%
-1.5%	B1R	0.0030	0.0025	17%	7.3	5.7	22%

627

**Table 8.** Concrete crack width.

Drift [%]	Bare [mm]	Retrofitted [mm]	Reduction [%]
-0.75	0.60	0.26	43
-1.0	0.63	0.42	67
-1.5	0.72	0.51	71

628

**Table 9.** Phase D stiffness comparison.

Frame condition	K [kN/mm]	$(K_{\text{elastic}} - K) / K_{\text{elastic}}$ [%]
Bare - elastic	9.59	0.0
Bare - 1 <sup>th</sup> fracture	8.15	15.0
Bare - 3 <sup>rd</sup> fractures	4.99	52.0
Rehabilitated - 1 <sup>st</sup> fracture	9.20	4.2
Rehabilitated - 3 <sup>th</sup> fractures	9.00	6.3

629

**Table 1.** Plate thicknesses for phase targets

	Phase A	Phase B	Phase C	Phase D
Drift [%]	0.75	3.0	3.5	4.0
Design targets	-15% $M_y^+$	-20% $\theta_p^+$	-0% V	> 80% $V_{bare,max}$
Design Plate [mm]	10	12	16	16
Plate tested [mm]	12	12	12	16

**Table 2.** Material properties

	$\sigma_y$ [Mpa]	$\sigma_u$ [Mpa]	$E$ [Mpa]
Flange	301	423	203,000
Web	372	441	204,000
Slab	24	32	24,808
Bending plate	311	450	217,000

**Table 3.** Overall frame behavior

	Bare	Retrofit	ratio
Elastic stiffness [kN/mm]	9.6	11.0	1.15
Yielding force [kN]	119	136	1.14
Second stiffness [kN/mm]	5.0	7.3	1.46
Maximum strength [kN]	250	320	1.28
Residual stiffness with fracture [kN/mm]	7.3	9.0	1.23
Residual strength with fracture [kN]	165	250	1.52

**Table 4.** Main loading points during test

Number	Phase	Loading Cycle (Drift)	Event
B1	A	0.50%	First beam end yielding (B1L, bottom)
R1	A to B	1.00%	Four beam ends yielding
R2	B to C	3.00%	First fracture (B2L, bottom)
B2	B	2.00%	Bare frame 1 <sup>st</sup> fracture
B3	C	1.65%	Residual drift
R3	C	-3.50%	Second fracture (B1L, top)
R4	D	-3.50%	MDAD failure (TR4)
B4	D	3.50%	Residual capacity
R5	D	4.00%	Recovered capacity

**Table 5.** Phase A: beam rotational stiffness and strength

Target 15% drift [%]	section	$K^+$ [kNm/rad]	$K^-$ [kNm/rad]	k	$M^+$ [kNm]		reduction
					Bare	MDAD	
0.75%	B1L	15,979	8,284	2.3	41	35	14%
	B2L	20,922	9,063	1.9	33	27	18%

**Table 6.** Frame stiffness

Drift [%]	Configuration	$K$ [kN/mm]	Ratio	$K_{sec}$ [kN/mm]	Ratio
1.0	Bare	9.9	—	—	—
	Retrofit	9.4	0.95	—	—
-1.0	Bare	9.9	—	—	—
	Retrofit	9.5	0.97	—	—
+1.5	Bare	10.0	—	5.0	—
	Retrofit	8.7	0.87	7.3	1.45
-1.5	Bare	8.9	—	5.5	-
	Retrofit	7.9	0.88	7.5	1.36

**Table 7.** Plastic rotation

Drift	section	$\theta_p$ [rad]			$\Sigma \theta_p / \theta_y$		
		Bare	MDAD	Red.	Bare	MDAD	Red.
1.5%	B1L	0.0070	0.0057	19%	11.0	7.7	30%
-1.5%	B1R	0.0030	0.0025	17%	7.3	5.7	22%

**Table 8.** Concrete crack width

Drift [%]	Bare [mm]	Retrofitted [mm]	Reduction [%]
-0.75	0.60	0.26	43
-1.0	0.63	0.42	67
-1.5	0.72	0.51	71

**Table 9.** Phase D stiffness comparison

Frame condition	$K$ [kN/mm]	$(K_{elastic}-K)/K_{elastic}$ [%]
Bare - elastic	9.59	0.0
Bare - 1 <sup>th</sup> fracture	8.15	15.0
Bare - 3 <sup>rd</sup> fractures	4.99	52.0
Rehabilitated - 1 <sup>st</sup> fracture	9.20	4.2
Rehabilitated - 3 <sup>th</sup> fractures	9.00	6.3

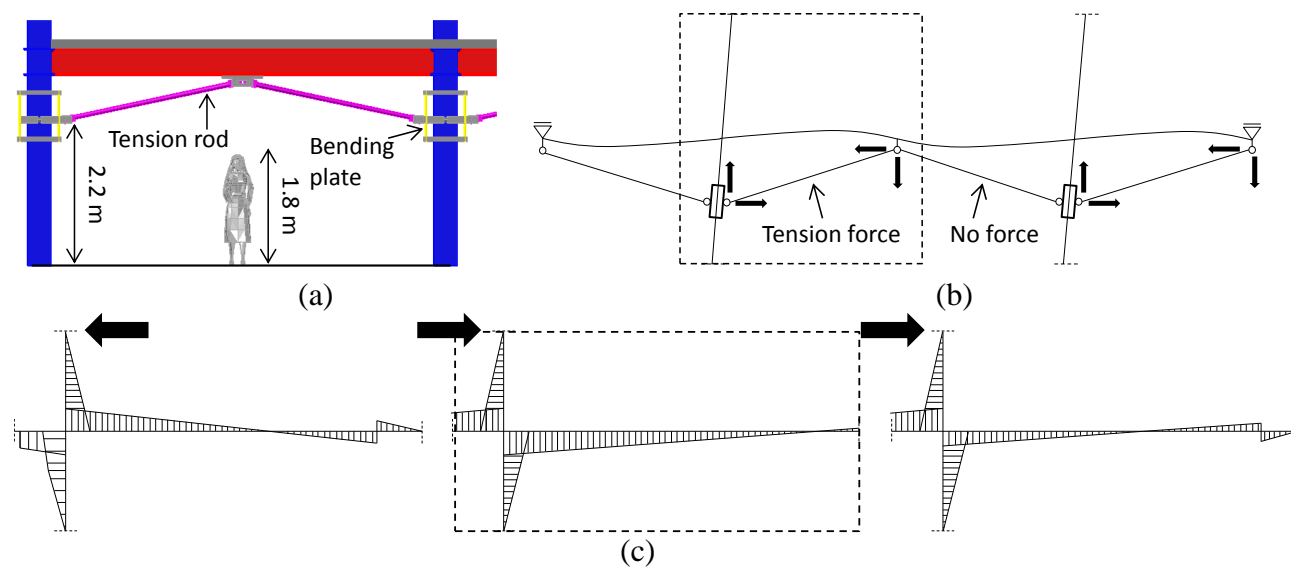


**Fig. 1.** MDAD configuration; a) minimal disturbance configuration; b) MDAD schematic mechanism; c) Moments distribution



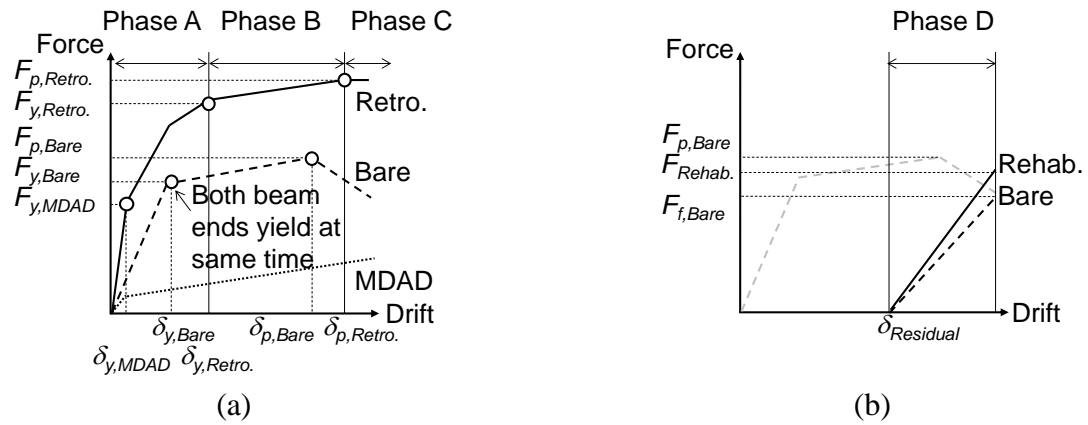


**Fig. 2.** Concept of multi damage-state retrofit; a) retrofit targets; b) rehabilitation target

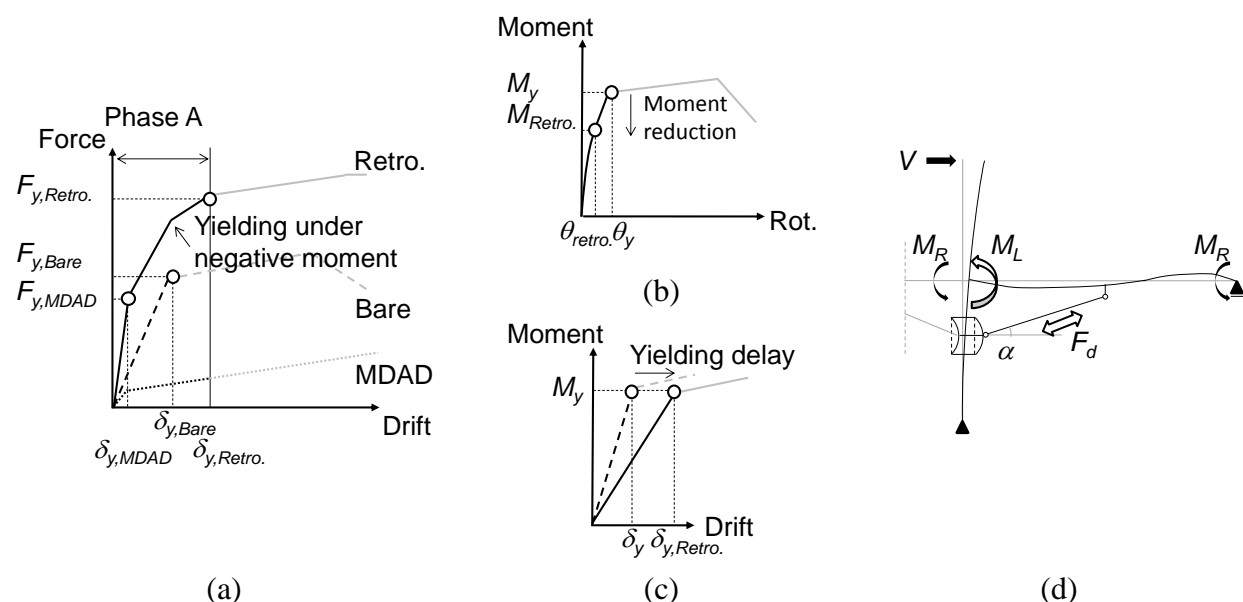


**Fig. 3.** Phase A design: a) force-drift relationship; b) moment-rotation relationship; c) plastic rotation-drift relationship; d) subassembly model

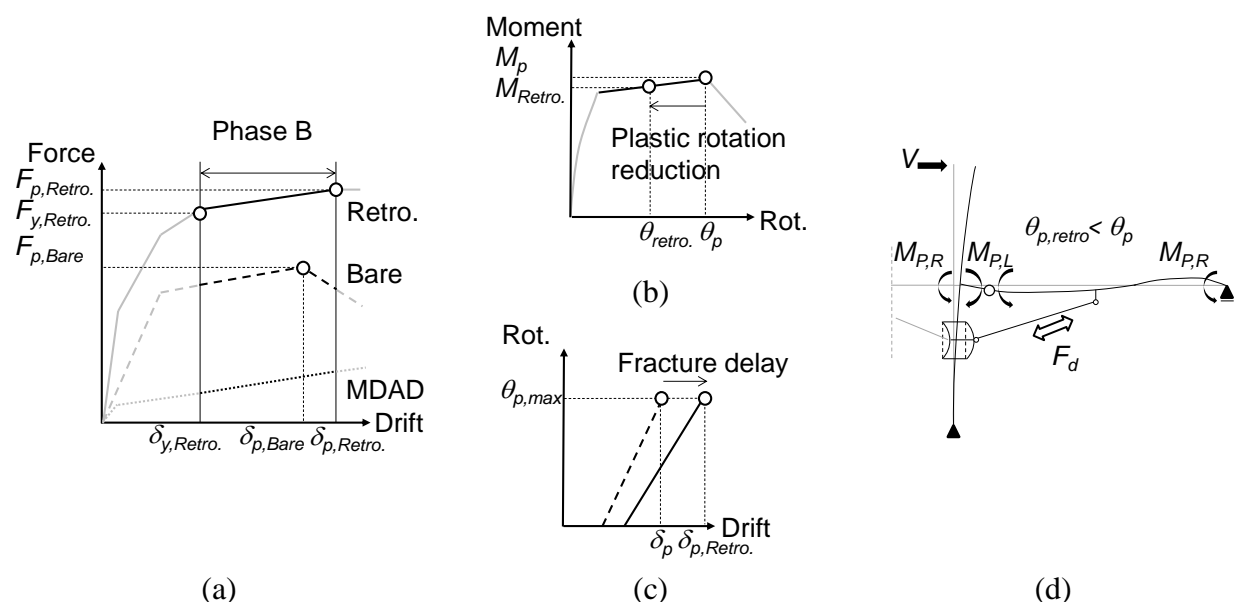


**Fig. 4.** Phase B design: a) force-drift relationship; b) moment-rotation relationship; c) plastic rotation-drift relationship; d) subassembly model

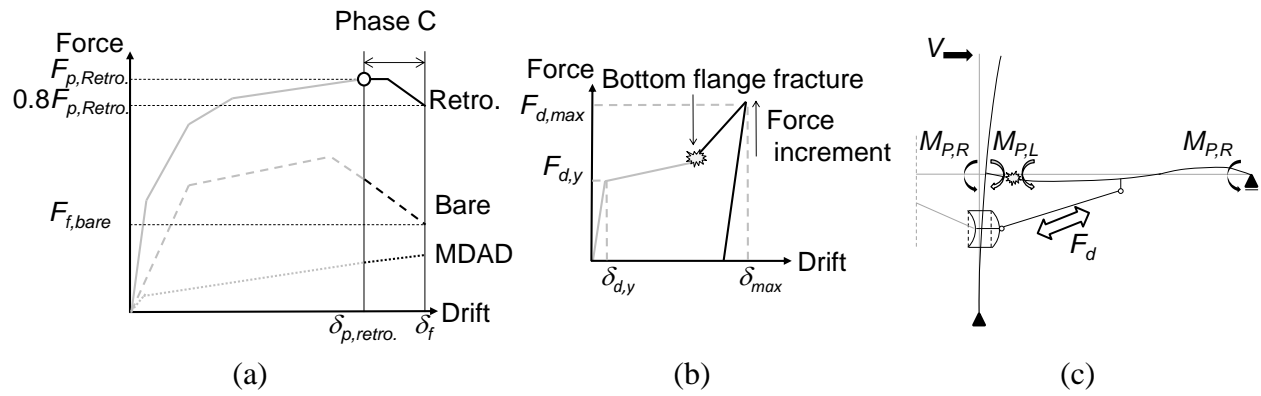


**Fig. 5.** Phase C design; a) force-drift relationship; b) tension rod force-drift relationship; c) subassembly model

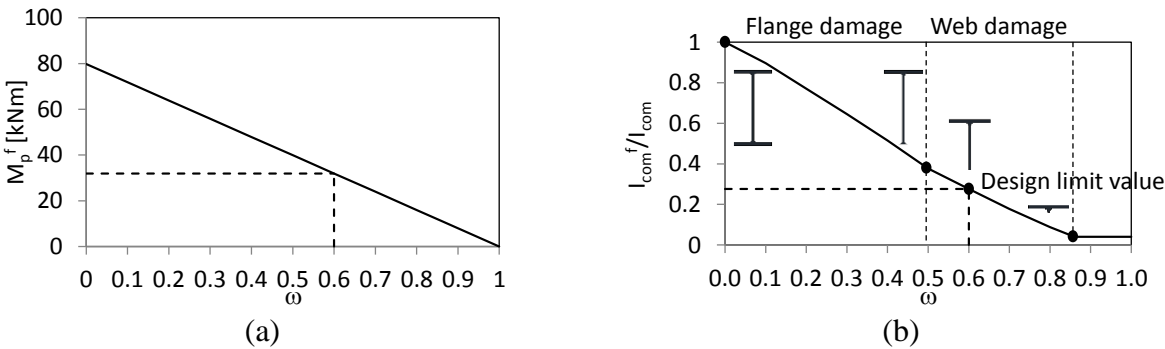


**Fig. 6.** Damage parameter for a) plastic moment; b) moment of inertia

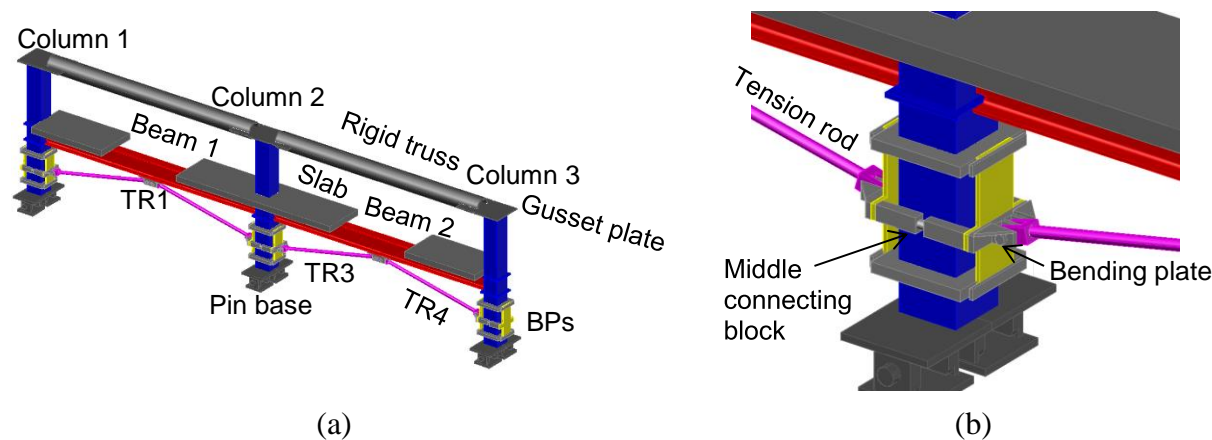


**Fig. 7.** Test specimen; a) 3D isometric view; b) internal MDAD

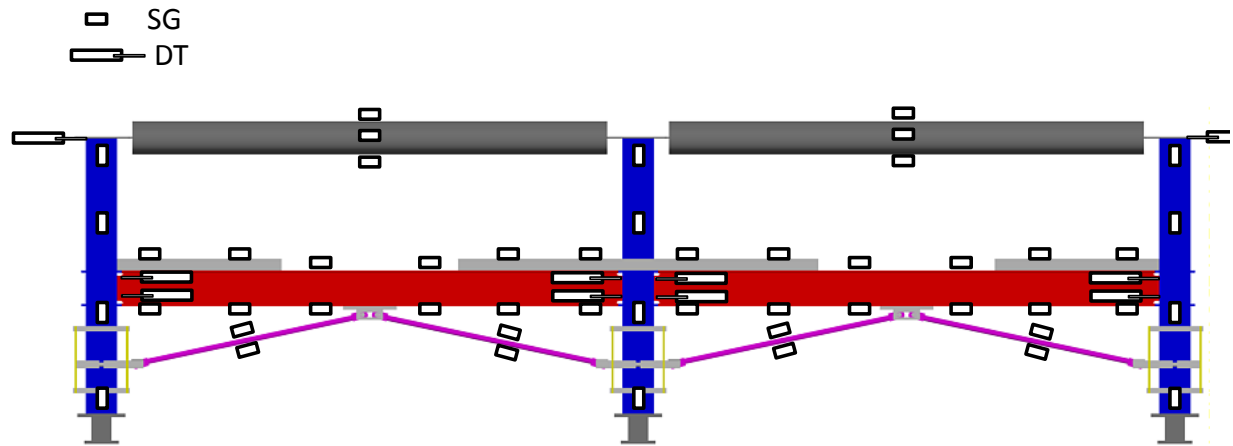


**Fig. 8.** Measurement system

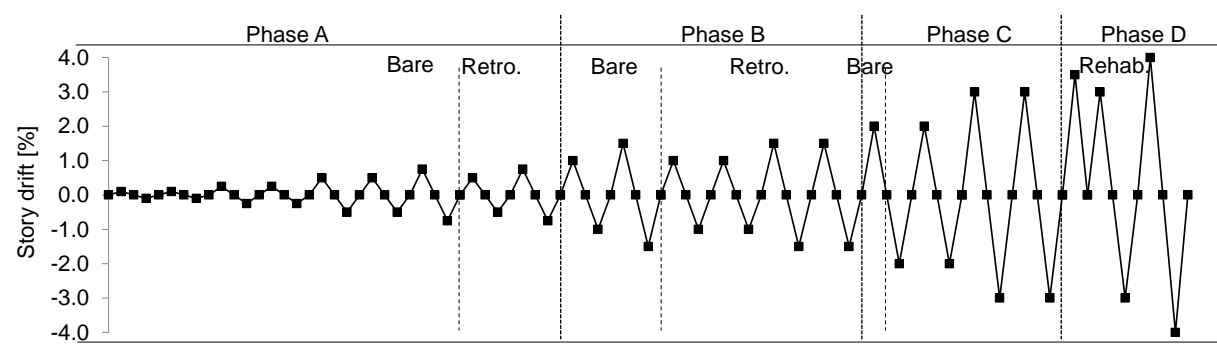
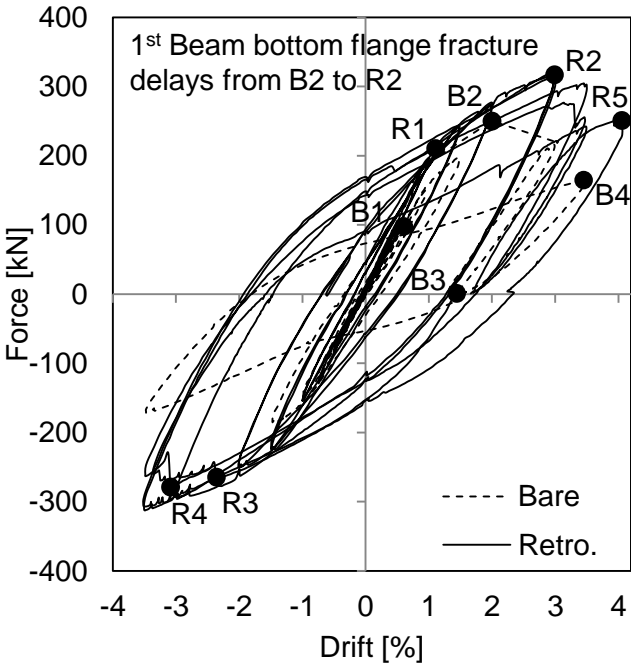
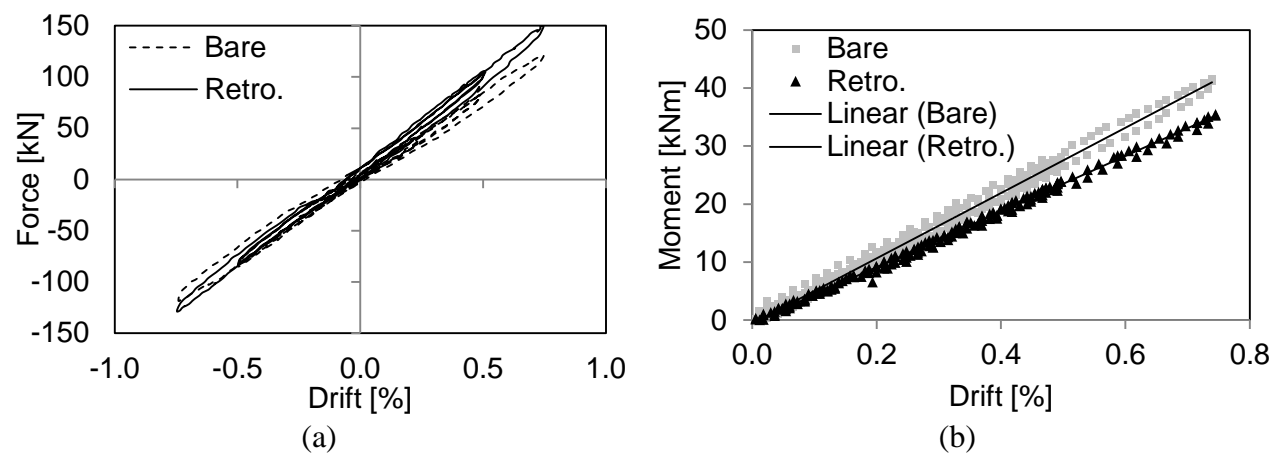


Fig. 9. Loading protocol





(a) (b)  
**Fig. 10.** Overall behavior; a) test frame before retrofit; b) frame hysteresis behaviour



**Fig. 11.** Phase A; a) frame hysteresis behavior; b) positive moment reduction at B1L

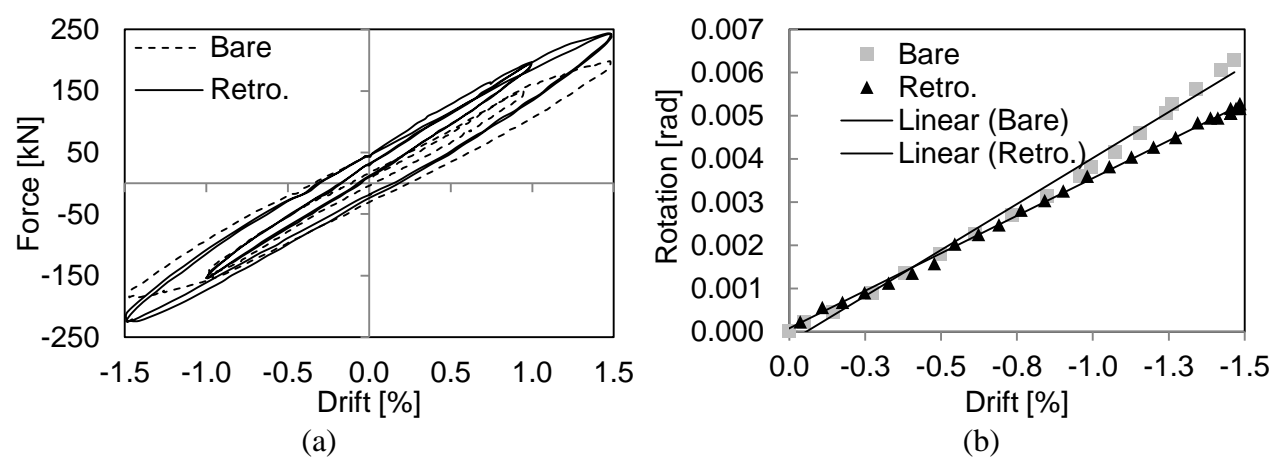


**Fig. 12.** Phase B; a) frame hysteresis behavior; b) positive plastic rotation reduction

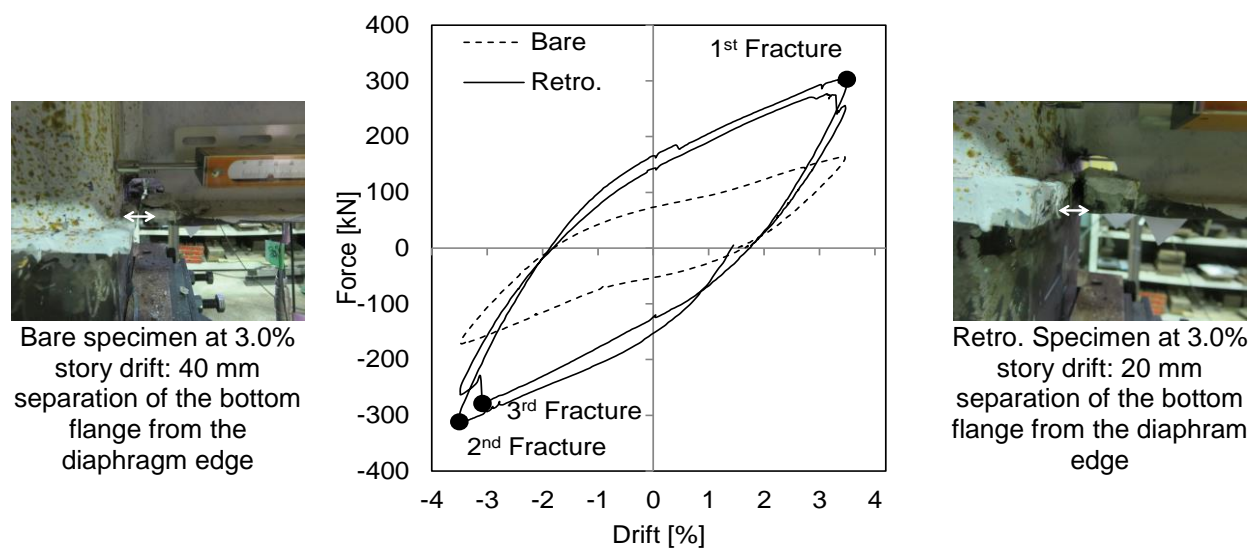


**Fig. 13.** Frame hysteresis behavior in phase C

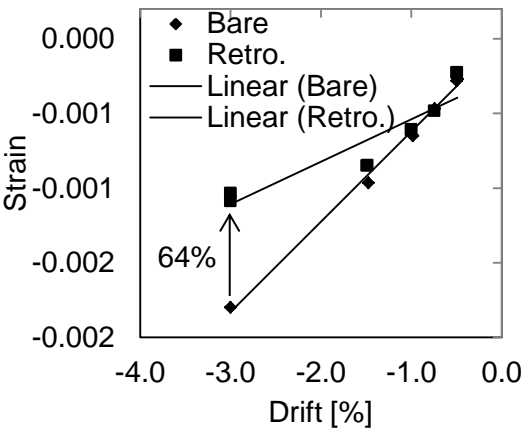


**Fig. 14.** Axial strain reduction at the beam end bottom flange under negative moment (B1L)

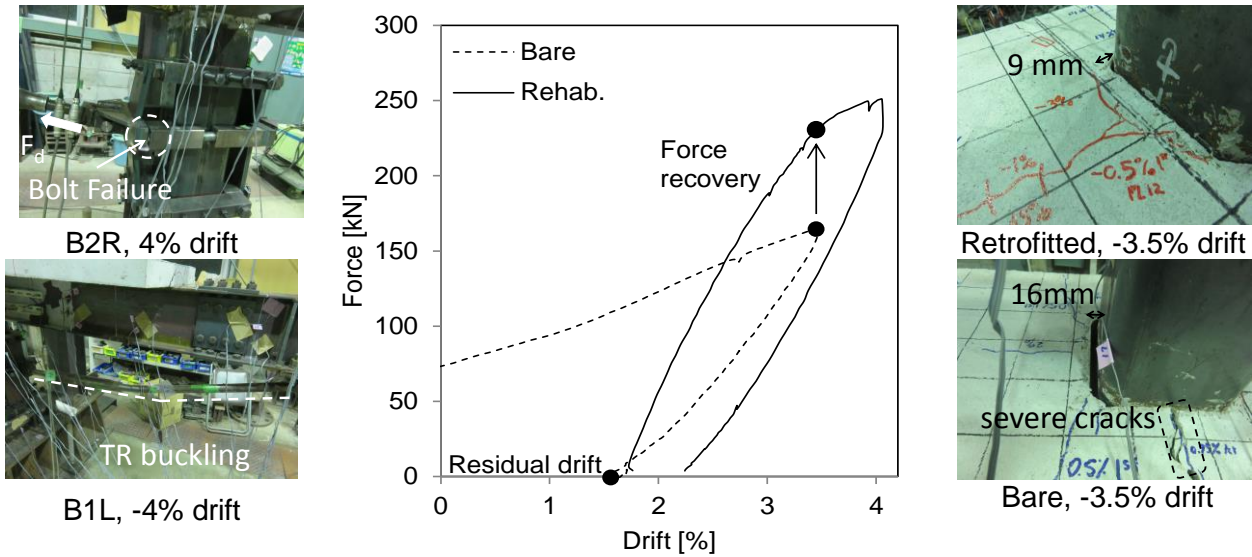


**Fig. 15.** Frame hysteresis behavior in phase D